TURBULENT MIXING OF A PASSIVE SCALAR IN GRID TURBULENCE

Y Ito*, T Watanabe, K Nagata, and Y Sakai

Dept. Mechanical Science and Engineering, Nagoya University
Chikusa-ku, Nagoya 4648603, Japan
*Corresponding: Tel/Fax: +81-52-789-4488; Email: yito@nagoya-u.jp

Abstract: Fractal grids have been attracted as a new-type of turbulence-generating grid due to their unique characteristics. Recent studies have revealed that such uniqueness appears in the near field of regular grid-generated turbulence. On the other hand, scalar transport in those flows is also of great interest but it has not been fully understood yet. In this study, therefore, we investigate the scalar mixing in the near field of regular grid-generated turbulence with various grid configurations. Experiments are carried out in liquid mixing layers with a Reynolds number of 5,000 based on the mesh size of the grid and uniform velocity. Simultaneous measurements of two-component velocities and a concentration are carried out by particle image velocimetry (PIV) and a planar laser-induced fluorescence (PLIF) technique, respectively. The results show that the scaling law using the wake-interaction length scale is applicable for the turbulence intensity in the grid turbulence with different mesh sizes. However, it is only partially applicable for the grid turbulence with different mesh sizes. Turbulence intensity increases with the thickness the grid bar and the scalar diffusion increases accordingly. The streamwise development of the scalar mixing layer thickness collapses into a single curve by normalizing by the thickness of the grid bar.

1. Introduction

Turbulent mixing and diffusion appear in wide variety of situations in both environmental and industrial flows [1]. They are usually driven by mean fluid shear as in jets and mixing layers [2,3,4,5] but there often exist that mixing and diffusion take place in a shear-less turbulent flow [6]. Modeling and scaling of such scalar transport are of great importance to predict those transport phenomena particularly from an applied point of view.

Regular turbulence-generating grids whose mesh size and thickness are fixed have been commonly used in fundamental turbulence researches because of their high level of isotropy and homogeneity. On the other hand, fractal grids, which a geometric pattern such as a square with different scales is superposed systematically, have been attracted as a new-type of turbulence generator [7]. Past experimental and numerical studies on fractal square grid turbulences revealed that the turbulent characteristics are very unique and differ from those of

regular grid turbulence [7-22]. Some of the features are: turbulence intensity in fractal grid turbulence is larger than that in regular grid turbulence with the same or higher blockage ratio [7-14]; the decay rate of the turbulence intensity is larger than that in regular grid turbulence [7-12]; the streamwise distributions of the integral length scale and Taylor's microscale stay almost constant along the centerline of the fractal grid whereas they usually increase with the streamwise distance [7-12,15,16]. These indicate that the fractal grids generate strong turbulent flows with large Reynolds numbers based on the Taylor's microscale. Furthermore, such characteristics have interpreted as non-equilibrium turbulence due to the fact that the dissipation rate constant, C_ε, ($=\varepsilon L/u'^3$ where ε is the decay rate of turbulent kinetic energy, L is the integral length scale, and u' is the RMS velocity) is not constant, meaning the flow does not follow the Richardson-Kolmogolov law [8-11,15,16]. From a scaling point of view, Mazellier and Vassilicos [9] introduced the wake-interaction length scale x_*,

$$x* = \frac{{L_0}^2}{t_0} \quad (1)$$

where L_0 and t_0 are the length and thickness of the biggest mesh of the fractal grid, respectively, and showed that it characterizes the flow structure in fractal grid turbulence well.

On the other hand, for deeper understanding of fractal grid turbulence, some researchers separated the fractal elements of the grid to investigate the roles of each element. Numerical studies by Zhou et al. [23,24] have focused on a flow downstream of a single square grid which corresponds to the largest grid of the fractal grid. In these studies, some turbulence characteristics agreed between the fractal and single square grid turbulences. For example, the streamwise location where turbulence intensity becomes the maximum is determined by the large-scale wake interactions in both grids. In other words, the largest grid plays a main role and the smaller grids are supplemental in fractal grid turbulence [24]. They also confirmed that the unusual high energy decay rate region observed in the past studies appears only in the near field of the fractal grid [24]. However, the above never means that the smaller grids are negligible. Zhou et al. [24] concluded that the smaller grids work as a quasi-background turbulence generator which contributes to several unique characteristics of fractal grid turbulence including the existence of non-equilibrium region. Here a single square grid resembles a part of a regular square-type grid in its form [24], so it is understandable that the non-equilibrium turbulence also appears in the near field of regular turbulence-generating grids [15]. In addition, Thormann et al. [17] have carried out wind tunnel experiments with several shapes of active fractal grids. They found some similarities between normal (passive) fractal turbulence and active fractal turbulence but some characteristics are rather closer to regular grid turbulence.

As shown above, a number of researches have been carried out to clarify the turbulence structure in fractal grid turbulence or non-equilibrium turbulence appearing in regular grid turbulence. On the other hand, scalar transport in such turbulences is also of great interest. Laizet and Vassilicos [18] showed that fractal grids enhance scalar transfer remarkably through a direct numerical simulation (DNS) study on turbulent mixing with

a linear scalar gradient. They also explained the reason by introducing space-scale unfolding (SSU) mechanism [13]. Cafiero et al. [20] have experimentally shown that a fractal grid significantly enhances diffusion of an impinging jet with respect to a regular grid with almost the same blockage ratio. Our experimental and numerical studies [14,19] on scalar mixing layer under non-premixed conditions revealed that the fractal grid enhances turbulent mixing more than a regular grid with the same porosity. It is basically due to the larger turbulence intensity in the fractal grid turbulence in comparison with the regular grid turbulence. These mixing and diffusion enhancement are also expected to be attributed to the nature of fractal grids that they generate wide spectrum of eddies, because scalar mixing is driven not only by large eddies that promote scalar diffusion at large scales but also by small eddies that promote local mixing at the fluids interfaces. However, the complexity of the configuration of fractal grids makes us hard to clarify which parameters of the grid determine scalar diffusion or which scale of eddies contributes to mixing. These are of great importance particularly in optimization and design of in-line static mixers making use of wakes.

In the present study, therefore, we experimentally investigated the turbulence structure and diffusion of a passive scalar in the near field of regular grid turbulence with various grid mesh size and thickness.

2. Experimental

Figure 1 shows a schematic of the experimental apparatus. The test section is the same as the one used in our previous studies [2,3,4]. It is a rectangular water tunnel made of polymethylemethacrylate (PMMA), whose size is 1.5 m in the streamwise length and 0.1 x 0.1 m^2 in cross section. A turbulence-generating grid is installed at the entrance to the test section (x = 0). Here the origin of the coordinates is the center of the entrance of the test section, and x, y, and z denote streamwise, vertical, and spanwise directions, respectively. The fluid used is filtered and dechlorinated tap water at a room temperature. Two separated flows are introduced to the test section as upper and lower streams under a non-premixed condition. As a passive scalar, a fluorescence dye, Rhodamine B, was initially premixed in the lower stream at a concentration, C_0, of 2.1 x 10^{-7} mol L^{-1}.

Table 1 lists the experimental conditions including grid configurations and initial flow conditions. In this paper, each flow type is referred as the first column of the Tab. 1 based on the grid configuration. All grids have a bi-plane configuration with a streamwise thickness of 10.0 mm. The mesh size, M, is varied from 22.36 mm to 28.87 mm and the thickness of the grid bar in the vertical and spanwise directions, t, is varied from 3.75 mm to 6.25 mm. Note that the porosity is the same for M25t4 and M29t5 cases and M25t6 and M22t5 cases. Also the central horizontal bar of the grid locates at y = 0 to mitigate the influence of the splitter plate which separates the upper and lower streams in the contract section. The uniform velocity, U_0, is set so as to achieve the Reynolds number based on the U_0 and M, Re = 5,000 for all the cases.

Instantaneous streamwise and vertical velocities and the concentration of Rhodamine B were measured by particle image velocimetry (PIV) and a planar laser-induced fluorescence (PLIF) technique, respectively. The central plane of the test section ($z = 0$) was illuminated by a Nd: Yag laser (wavelength: 532 nm) sheet with a thickness of 1 mm at a power of 3W. The laser sheet was parallelized by two convex lenses and introduced from the bottom wall of the test section in the vertical (y) direction. Polystyrene particles with a typical diameter of 11 μm are dispersed in the flow as tracers. For imaging, two high-speed video cameras (Ametek Phantom V210) were placed on the both sides of the test section. They were aligned symmetrically against the test section so that their imaging areas match exactly. A band-pass filter (wavelength: 532 nm) and long-pass filter (wavelength: 580 nm) were attached in front of each camera lenses for the PIV and PLIF, respectively. The resolution of the captured images is 128 pixel x 800 pixel for an area of 16 mm x 100 mm. Post processing for calculating the velocities by PIV was carried out using commercial software (DANTEC Dynamic Studio). Typical interrogation area was set to 16 x 16 pixels with an overlap of 50%, resulting the spatial resolution of 1 mm. On the other hand, a lab-made program developed by Suzuki et al [14] was applied to calculate the instantaneous concentration of Rhodamine B. The data is typically acquired at a sampling frequency of 500 Hz for 16 seconds. Measurements were carried out at the central plane of the test section ($z = 0$) in the range of 80 mm < x < 300 mm ($3.2 < x/M < 12.0$ for M25t5 case) and -50 mm < y < 50 mm ($-2.0 < y/M < 2.0$ for M25t5 case).

3. Results

3.1 Velocity field

Figure 2 shows the vertical distributions of the local mean velocity, $\langle U \rangle$, for M25t5 case. Here, <*XX*> denotes a time-averaged value of *XX* and *U* is normalized by the initial velocity, U_0. There are clear velocity defects due to the grid in the upstream region but the mean velocity distribution in the region of $-1 < y/M < 1$ becomes almost uniform in the downstream region of $x/M > 7$. $\langle U \rangle / U_0$ in the downstream region is slightly greater than 1 because of the boundary layer development along the channel walls.

Figure 3 shows the vertical distributions of the mean-squared streamwise and vertical velocity fluctuations, $\langle u^2 \rangle$ and $\langle v^2 \rangle$, for M25t5 case. Here they are normalized by $\langle U \rangle^2$. In common with the mean velocity distribution, the velocity fluctuations approach uniform while decaying in the downstream direction. The other four cases basically show the similar tendency in both the mean velocity and velocity fluctuation distributions.

Figure 4 shows the streamwise distributions of $\langle u^2 \rangle / \langle U \rangle^2$ and Fig. 5 shows the ratio of the RMS velocities in the streamwise and vertical directions, $u_{rms} / v_{rms} \left(= \sqrt{\langle u^2 \rangle} / \sqrt{\langle v^2 \rangle} \right)$, both at the centerline. We first notice that, by comparing M25t4, M25t5, and M25t6 cases, turbulence intensity increases with the thickness of the grid bar, *t*. The influence of the mesh size, *M*, on the other hand, is not clear but relatively small. From a different aspect, the distributions for M25t4 and M29t5 cases or M25t6 and M22t5 cases are not the same, meaning that the porosity of the grid is not a decisive parameter. In Fig. 5, we see the values of u_{rms} / v_{rms} lie around 1 in the measured region in all the cases. These indicate that the flows have relatively good homogeneity and isotropy as in conventional grid-generated turbulences.

The mean-squared velocity fluctuation in grid-generated turbulence follows a power decay law defined by the following equation,

$$\frac{\langle u^2 \rangle}{\langle U \rangle^2} = a \left(\frac{x - x_0}{M} \right)^{-n}. \quad (2)$$

Here *n* is the decay rate, *a* is a constant, and x_0 is the virtual origin. The calculated *n* for the present flows with an assumption that x_0 is 0 [11] is shown in Table. 2. As in Tab. 2, *n* in the present study lies 1.35—1.94. The typical value of *n* in regular grid turbulence is around 1.2 [25], and the theoretical value is 6/5 for Saffman turbulence and 10/7 for Batchelor turbulence [25]. On the other hand, *n* in fractal grid turbulence and regular grid turbulence in the vicinity of the grid takes larger values of 1.6—1.9 [11,23,25]. Hence it is confirmed that the decay rate of turbulence intensity in the present study is close to that of fractal grid turbulence.

It has been reported that the turbulence intensity in fractal grid turbulence collapses into a single curve when the streamwise location, *x*, is normalized by the wake-interaction length scale, x_*. To investigate the applicability of this scaling law to the present experiments, $\langle u^2 \rangle / \langle U \rangle^2$ is replotted against x/x_* in Fig. 6. Note that *M* and *t* are used as L_0 and t_0, respectively, in Eq. (1) because regular grids are employed in this study. Figure 6 illustrates that the distributions for M25t5, M22t5, and M29t5 cases collapse into a single curve, i.e., both decay exponent, *n*, and constant, *a*, are identical, but *n* is smaller and *a* is larger for M25t6 case, in which the thickness of the grid bar is thicker, and *n* is larger and *a* is smaller for M25t4 case. In other words, the scaling law using x_* is partially applicable. Discussion on *n* and *a* includes the controversy on virtual origin, x_0, so the followings may be limited to the present analysis but our results illustrate that, in the vicinity of the grid, the decay exponent depends on the thickness of the grid bar, *t*. Also, *a* is directly related to turbulence intensity. Therefore *t* or the local Reynolds number based on the uniform velocity and thickness of the grid bar, Re_t, may play important roles on both *n* and *a* in the near field of grid turbulence.

3.2 Scalar field

Figure 7 shows the vertical distributions of the mean concentration, $\langle C \rangle$, for M25t5 case. Here C is normalized by the initial concentration, C_0. It is confirmed that the distribution is almost symmetric about the centerline and the scalar mixing layer thickness develops toward the downstream direction. To quantitatively evaluate the scalar diffusion, the concentration mixing layer thickness, δ, was calculated. Here δ is defined by [27]

$$\delta = y_{<C>=0.25} - y_{<C>=0.75}. \quad (3)$$

Figure 8 shows the streamwise development of δ. Among the tested cases, δ is the largest for M25t6 case and smallest for M25t4 case. This result reflects the magnitude order of the turbulence intensity. As well as the velocity profile, the effect of the mesh size of the grid is not very clear and in fact the development of δ is almost the same for M25t5, M22t5, and M29t5 cases.

As mentioned, while active discussion has been carried out for the velocity field in non-equilibrium turbulences and several scaling laws using parameters such as x_* and the effective mesh size of the grid, M_{eff} ($= \frac{4T^2}{P_M}(1-\sigma)$, where T^2 is the cross-sectional area of the channel and P_M is the fractal perimeter's length of the grid, and σ is the blockage ratio) [8], no scaling law has been proposed for scalar in the near field of regular grid turbulence. It is obvious from the data shown above that x_* does not characterize the mixing. Here on the basis of the obtained results that the effect of t is large, the mixing layer thickness was normalized by t in Fig. 9. Interestingly the distributions became almost identical for all the cases including the different t cases. We unfortunately have not come up with a theoretical backup for this scaling law and it needs to be carefully investigated further in the future, but considering that the turbulence intensity increases with t, this result is reasonable. On the other hand, assuming evolution of scalar diffusion for statistically stationary turbulence, we obtain the following relationship between the mixing layer thickness and streamwise distance [28,29]:

$$\delta \propto \sqrt{\frac{x}{M}}. \quad (4)$$

Thus we replotted the data in log-log coordinates in Fig. 10. Since the mixing layer thickness is a summation of diffused scalar in the upstream region, the nature is different from energy dissipation and it is not surprising that it does not become a single straight line. Instead, it can be divided into the region; $x/M<5$ and $x/M>5$. The straight line in Fig. 10 corresponds to $n=0.5$. It is found that it aligns well with the plots in the region of $x/M>5$. In other words, except the very near region of the grid, the development of mixing layer thickness follows the conventional diffusion process.

Also, it is known that the integral length scale, L,

$$L(x) = \int_0^\infty \frac{<u(x)u(x+r)>}{<u(x)^2>} \mathrm{d}r, \quad (5)$$

represents the scale of large eddy of turbulence and it is supposed to be highly related to scalar diffusion. Therefore, L of the streamwise velocity in the longitudinal direction was calculated using the Taylor's frozen turbulence hypothesis for the M25t5, M25t4, and M25t6 cases. Figure 11 shows the results along the centerline. Here L is normalized by M. The line corresponds to the Saffman turbulence. Although the data is scattering, the magnitude order of L is generally M25t6>M25t5>M25t4 which is the same as that of t and u'. Thus we can conclude that a regular grid with a larger thickness of the grid bar generates stronger turbulence with a larger integral length scale and it enhances scalar diffusion.

Simultaneous measurements of the velocities and concentration allow us to calculate the cross-correlation terms such as the turbulent scalar flux. This is an important parameter in modeling of scalar diffusion. Figure 12 shows the streamwise distributions of the vertical turbulent scalar flux, $\langle vc \rangle$, at the centerline. Here $\langle vc \rangle$ is normalized by $\langle U \rangle$ and C_0. The results basically reflect the magnitude order of the mixing layer thickness and the vertical scalar flux increases with the thickness of the grid bar, t. However, $\langle vc \rangle$ for M29t5 case is larger than that for M25t5 case particularly in the upstream region despite that the mixing layer thickness is almost the same between the two cases. We think this is caused by the difference of the vertical scalar diffusion in the region of $0 < x/M < 3$. In fact $\langle vc \rangle$ at $x/M = 2.6$ is smaller than that at $x/M = 3$ for M29t5 case whereas it keeps increasing toward the upstream direction in the other cases.

4. Conclusion

Turbulent mixing of a passive scalar in the near field of regular grid-generated turbulence is experimentally investigated. The main results are summarized as follows.

1) The wake-interaction length scale well characterizes the turbulence intensity distribution in the near field of grid turbulences with different mesh sizes. However, the scaling law is only partially applicable for cases with different thicknesses of the grid bar.

2) Both turbulence intensity and integral length scale increase with the thickness of the grid bar, and therefore, the scalar diffusion increases accordingly.

3) The streamwise distribution of the mixing layer thickness collapses into a single curve by normalizing the thickness of the grid bar. Except the very near region from the grid, the streamwise development of mixing layer thickness follows the conventional diffusion process.

Although a few questions remain and further investigation is required, the present study shows a new scaling law for a passive scalar, which would be beneficial for modeling too. We believe it is a good starting point to understand the scalar transport mechanism in the near field or non-equilibrium region of grid turbulences.

References

[1] Dimotakis P, Annu. Rev. Fluid Mech., 37, 329-356, 2005.

[2] Ito Y, Nagata K, Sakai Y, and Terashima O, Exp. Therm. Fluid Sci., 51, 28-36, 2013.

[3] Ito Y, Sakai Y, and Nagata K, Chem. Eng. Tech., 37, 2103-2108, 2014.

[4] Ito Y, Nagata K, and Sakai Y, Exp. Therm. Fluid Sci., 55, 166-173, 2014.

[5] Sakai Y, Watanabe T, Kamohara S, Kushida T, and I. Nakamura, Int. J. Heat Fluid Flow, 22, 227–236, 2001.

[6] Nagata K and Komori S, J. Fluid Mech., 430, 361-380, 2001.

[7] Hurst D and Vassilicos J C, Phys. Fluids, 19, 035103, 2007.

[8] Seoud, R E and Vassilicos, J C, Phys. Fluids, 19, 105108, 2007.

[9] Mazellier N and Vassilicos J C, Phys. Fluids, 22, 075101, 2010.

[10] Gomes-Fernandes R, Ganapathisubramani B, and Vassilicos J C, J. Fluid Mech., 94, 1-31, 2012.

[11] Valente P and Vassilicos J C, J. Fluid Mech., 744, 5-37, 2014.

[12] Laizet S and Vassilicos J C, Flow, Turbulence and Combust., 87, 673-705, 2011.

[13] Laizet S and Vassilicos J C, Phys. Rev. E, 86, 046302, 2012.

[14] Suzuki H, Nagata K, Sakai Y, and Ukai R, Physica Scripta, T142, 014069, 2010.

[15] Valente P and Vassilicos J C, Phys. Rev. Let., 108, 214503, 2012.

[16] Nagata K, Sakai Y, Inaba T, Suzuki H(iroki), Terashima O, and Suzuki H(iroyuki), Phys. Fluids, 25, 065102, 2013.

[17] Thormann A and Meneveau C, Phys. Fluids, 26, 025112, 2014.

[18] Laizet S and Vassilicos J C, J. Fluid Mech., 764, 52-75, 2015.

[19] Suzuki H, Nagata K, Sakai Y, and Hayase T, Physica Scripta, T142, 014065, 2010.

[20] Cafiero G, Discetti S, and Astarita T, Int. J. Heat Mass Trans., 75, 173–183, 2014.

[21] Hearsta1 R J and Lavoie P, J. Fluid Mech., 741, 567-584, 2014.

[22] Discetti S, Ziskin I B, Astarita T, Adrian R J, and Prestridge K P, Fluid Dyn. Res., 45, 061401, 2013.

[23] Zhou Y, Nagata K, Sakai Y, Suzuki H, Ito Y, Terashima O, and Hayase T, Phys. Fluids, 26, 045102, 2014.

[24] Zhou Y, Nagata K, Sakai Y, Suzuki H, Ito Y, Terashima O, and Hayase T, Phys. Fluids, 26 075105, 2014.

[25] Kitamura T, Nagata K, Sakai Y, Sasoh A, Terashima O, Saito H, and Harasaki T, J. Fluid Mech., 738, 378-406, 2014.

[26] Komori S, Nagata K, Kanzaki T, and Murakami Y., AIChE J., 39, 1611-1620, 1993.

[27] Jayesh and Warhaft Z., J. Fluid Mech., 277, 23-54, 1994.

[28] Libby P A, Acta Astronaut, 2, 867–878, 1975.

[29] Sakai Y, Nagata K, Suzuki H, Ito Y, Mixing and diffusion in regular/fractal grid turbulence, in Fractal Flow Design: How to Design Bespoke Turbulence and Why, CISM Courses and Lectures, 568, edited by Y. Sakai and J.C. Vassilicos, Springer-Verlarg, 2016.

Acknowledgement

Part of this study was supported by the Ministry of Education, Culture, Sports, Science and Technology, Japan, through Grants-in-Aid (Nos. 25289030 and 25289031).

Table 1. Grid configurations.

Flow type	Mesh size M (mm)	Thickness of the grid bar t (mm)	Wake-interaction length scale $x_*(=M^2/t)$ (mm)	Porosity (%)	Initial velocity U_0 (m s^{-1})	Re_M	Re_t
M25t5	25	5	125	64	0.26	5,000	1,000
M25t4	25	3.75	167	72	0.26	5,000	750
M25t6	25	6.25	100	56	0.26	5,000	1,250
M22t5	22.36	5	100	56	0.29	5,000	1,000
M29t5	28.87	5	167	72	0.22	5,000	1,000

Table 2. The power low decay rate and constant.

Flow type	Decay rate (n)	Constant (a)
M25t5	1.68	0.24
M25t4	1.94	0.59
M25t6	1.36	0.06
M22t5	1.35	0.16
M29t5	1.45	0.14

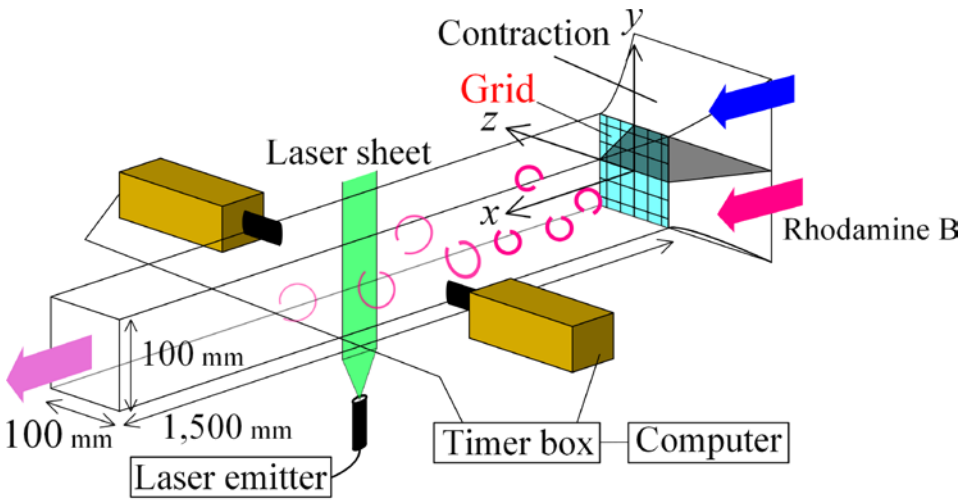

Fig. 1 Schematic of the experimental apparatus.

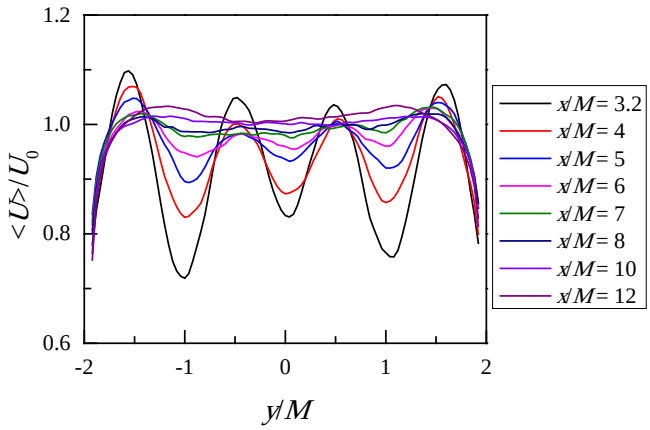

Fig. 2. Vertical distributions of the mean velocity for M25t5 case. There are clear velocity defects due to the grid in the upstream region but the mean velocity distribution in the region of $-1 < y/M < 1$ becomes almost uniform in the downstream region of $x/M > 7$.

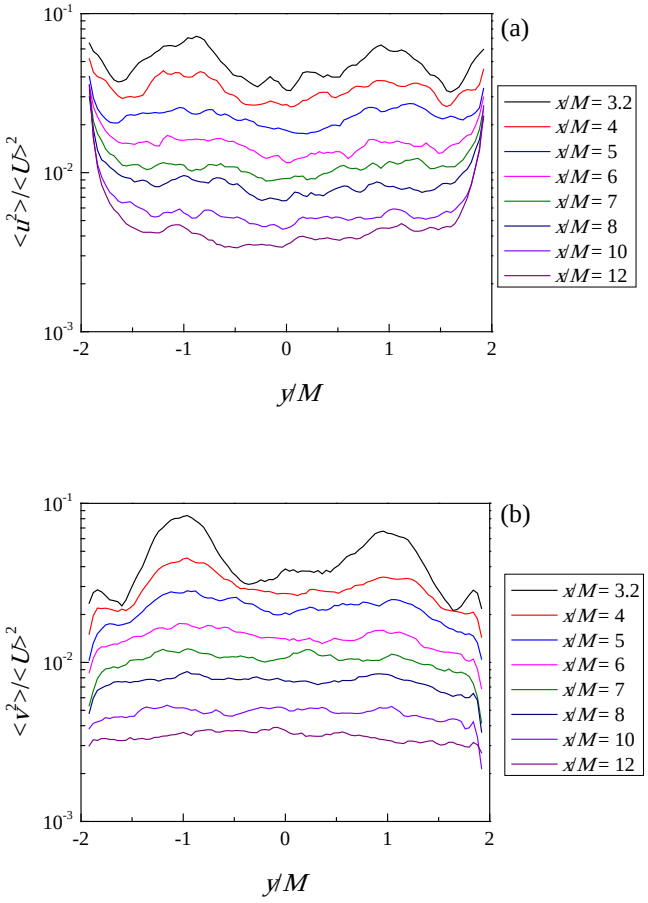

Fig. 3. Vertical distributions of the mean-squared (a) streamwise and (b) vertical velocity fluctuations for M25t5 case. The velocity fluctuations approach uniform while decaying in the downstream direction

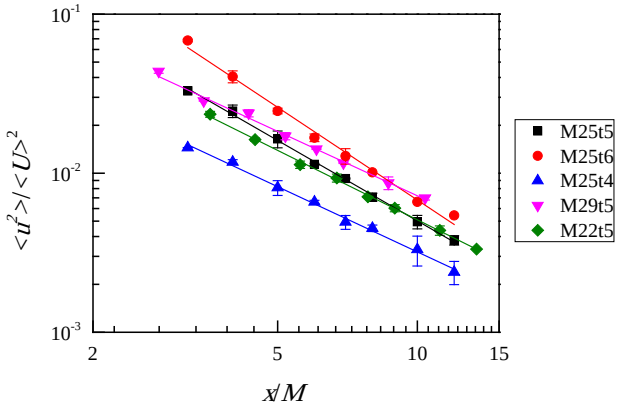

Fig. 4. Streamwise distributions of the mean-squared streamwise velocity fluctuation at the centerline. The *x*-axis is normalized by the mesh size. Turbulence intensity increases with the thickness of the grid bar, *t*. The influence of the mesh size, *M*, on the other hand, is relatively small.

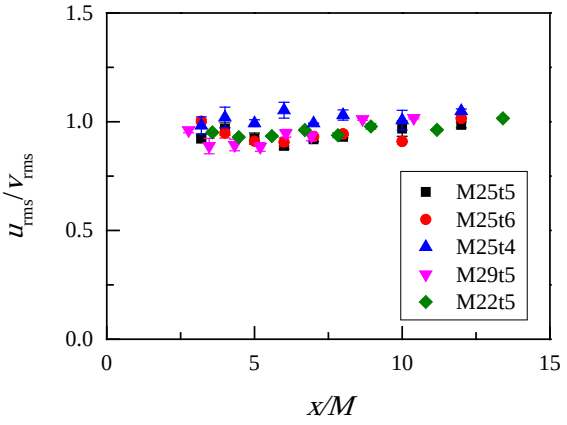

Fig. 5. Ratio of the RMS velocities in the streamwise and vertical directions. The flows have relatively good homogeneity and isotropy as in conventional grid-generated turbulences

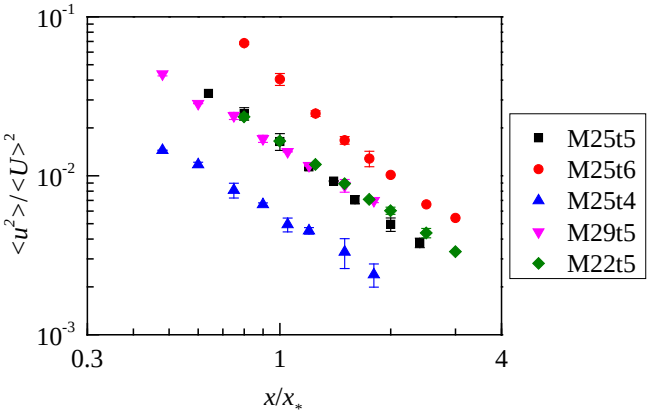

Fig. 6. Streamwise distributions of the mean-squared streamwise velocity fluctuation at the centerline. The *x*-axis is normalized by the wake-interaction length scale, x_*. The scaling law using x_* is applicable for the same mesh size case.

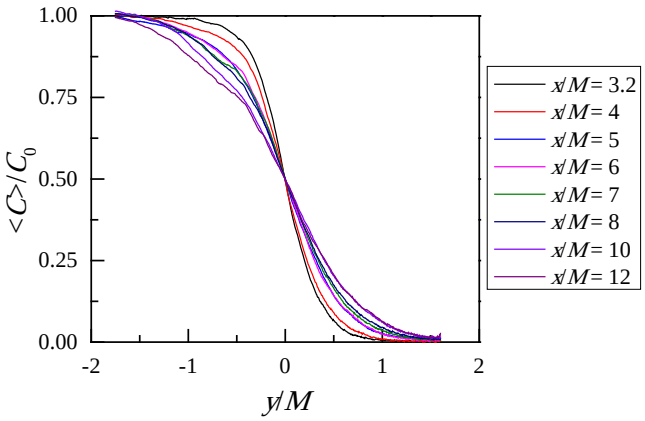

Fig. 7. Vertical distributions of the mean concentration for M25t5 case. It is confirmed that the distribution is almost symmetric about the centerline and the scalar mixing layer thickness develops toward the downstream direction.

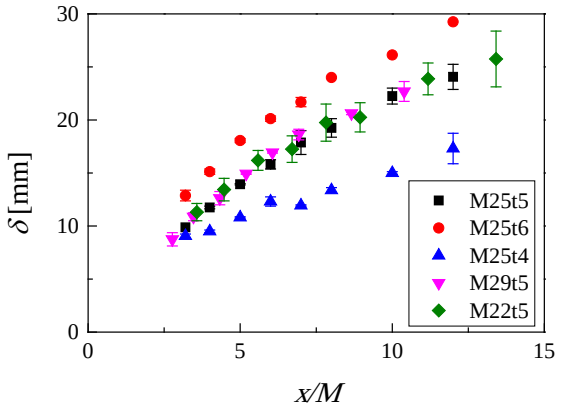

Fig. 8. Streamwise development of the concentration mixing layer thickness, δ. δ is the largest for M25t6 case and smallest for M25t4 case.

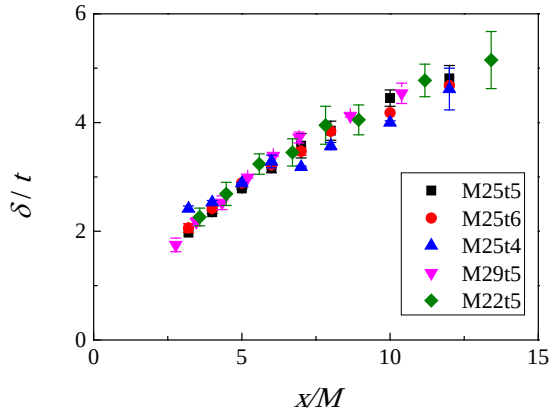

Fig. 9. Streamwise development of the concentration mixing layer thickness normalized by the thickness of the grid bar. The distributions are almost identical for all the cases.

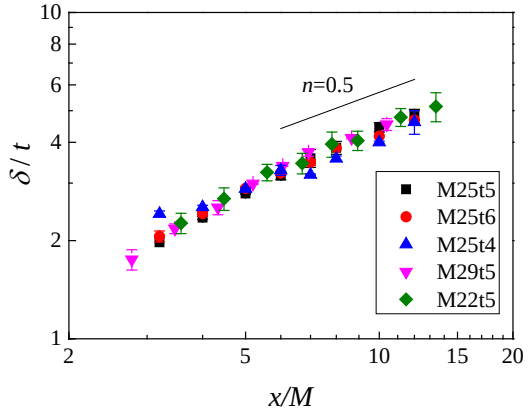

Fig. 10. Streamwise development of the concentration mixing layer thickness normalized by the thickness of the grid bar (in log-log coordinates). Except the very near region of the grid, the development of mixing layer thickness follows the conventional diffusion process following n=0.5.

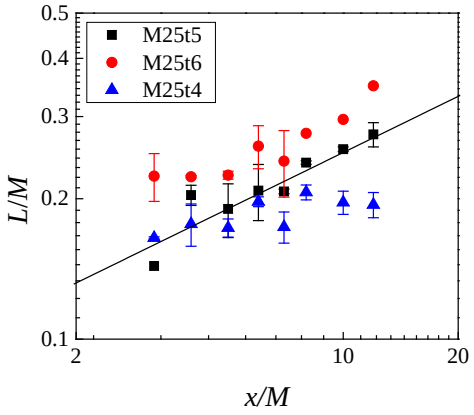

Fig. 11. Streamwise distribution of the integral length scale along the centerline. This figure indicates that a regular grid with a larger thickness of the grid bar generates stronger turbulence with a larger integral length scale.

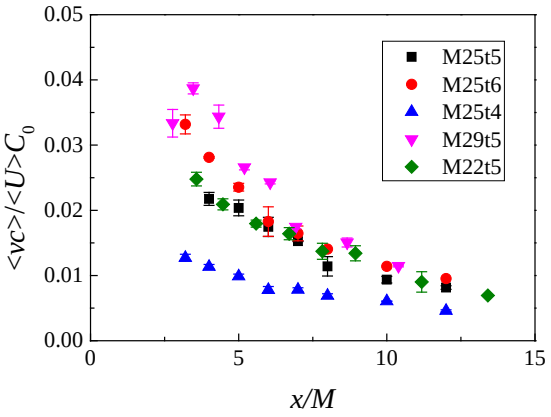

Fig. 12. Streamwise distribution of the vertical turbulent scalar flux at the centerline. The results basically reflect the magnitude order of the mixing layer thickness.